CFD simulations of a suspension bridge deck for different deck shapes with railings and vortex mitigating devices

View the article online for updates and enhancements.

CFD simulations of a suspension bridge deck for different deck shapes with railings and vortex mitigating devices

I Kusano[1*], J B Jakobsen[1] and J T Snæbjörnsson[1, 2]

[1] University of Stavanger, Stavanger, Norway
[2] Reykjavik University, Reykjavík, Iceland

[*] Corresponding author: ibuki.kusano@uis.no

Abstract. Aerodynamic response of a single-box suspension bridge girder is investigated using CFD simulations. The importance of including railings and vortex mitigating devices such as guide vanes and a spoiler in the simulations is explored since they alter the flow field around the deck greatly. The paper compares results from a bare deck section and a section with mitigating devices. A clear vortex shedding observed for the bare deck section is suppressed by the use of mitigating devices and the aerodynamic force coefficients are very different between these cases. The effect of varying deck width is also studied. Flutter derivatives are defined based on quasi-steady formulation and flutter velocity is computed for each section. The section with the largest width to depth ratio has the best performance against flutter. This study is an initial phase of multi-fidelity optimization of bridge deck shape considering aerodynamic constraints.

1. Introduction

With the advance of technologies, the achievable span of suspension bridges becomes longer and longer. The Great Belt Bridge and Akashi Bridge, which both opened in 1998, have main span of more than 1.6 km. Other suspension bridges, such as Xihoumen Bridge in China, which opened in 2009 and the recent construction of Osman Gazi Bridge in Turkey follow this trend. As the structures become longer and more flexible, they are more vulnerable to wind-induced phenomena such as flutter, buffeting and vortex shedding.

For the design of such structures, it is essential to consider their aerodynamic response, since it may lead to collapse. The shape of a bridge deck is one of the key factors influencing the structural response under wind load. Among different deck shapes, the stream-lined single box girder has become popular after its successful application to the Severn Bridge in UK in 1966. It possesses good performance against vortex shedding and flutter instabilities. Since the box section provides larger torsional inertia than open sections, the deck can be designed shorter in height, which results in more slender and aesthetic appearances. The box section is also more economic in construction as well as corrosion maintenance [1].

The characterization of aerodynamic response of a bridge deck has been historically performed in wind tunnel tests. However, according to Mannini at al. [2], Sarkic et al [3] among others, the improvement in Computational Fluid Dynamics (CFD) techniques in the last decade has made this method more increasingly reliable to study aerodynamic behaviour of bridge deck cross sections. For instance, Ge and Xian [4] used this technique to obtain flutter response of a bridge numerically.

This work focuses on the use of 2D unsteady Reynolds Averaged Navier-Stokes (URANS) CFD simulations to obtain aerodynamic coefficients for different deck shapes. Although this method presents some limitations such as perfect correlation of the flow along the span-wise direction, it can accurately provide the mean pressure distribution around the geometry and consequently force coefficients as demonstrated by researchers such as Vairo [5], Brusiani [6] and Nieto [7].

The aerodynamic coefficients are essential to characterize bridge deck section since they can be used to carry out flutter and buffeting analyses based on quasi-steady theory. This formulation is appropriate for high reduced wind velocities and streamlined deck cross sections according to Wu and Kareem [8] and Tubino [9].

In this work, the aerodynamic chatacteristics of different deck sections are studied. First of all, two deck sections, one with a bare deck and a second one with vortex mitigating devices are studied and compared. Then four sections of different deck width and a constant height are investigated. Flutter derivatives based on the evaluated force coefficients are compared as well as the flutter speed for each section. Although many researchers have worked with CFD simulation of a bare deck [10,11,12], there are are limited number of numerical investigations of deck sections with vortex mitigating devices [13,14,15]. Some previous studies have addressed the influence of aerodynamic appendages such as flaps on flutter velocity [16] or porosity of railings on critical flutter velocity [17].

This study is an initial phase of multi-fidelity optimization of a suspension bridge deck shape under flutter constraint. Julsundet Bridge in Norway was used as an application example.

2. Formulation

2.1 Force coefficients
The aerodynamic force coefficients and Strouhal number of a bridge deck section under wind load are expressed as:

$$C_L = \frac{L}{0.5 \cdot \rho U^2 B}; \quad C_D = \frac{D}{0.5 \cdot \rho U^2 H}; \quad C_M = \frac{M}{0.5 \cdot \rho U^2 B^2}; \quad S_t = \frac{fH}{U} \tag{1}$$

where C_L, C_D and C_M are lift, drag and moment coefficients, L, D and M are the time-averaged lift and drag forces and moment per unit of length, ρ is the flow density, U is the undisturbed wind velocity, f is the vortex shedding frequency and B and H are the width and the height of the deck cross-section. The force and sign convention used for the study is shown in Figure 1.
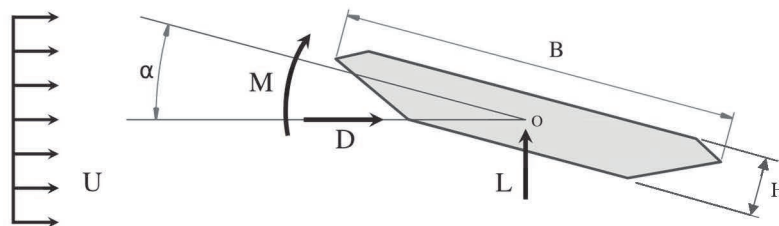
Figure 1. Force and sign convention of a bridge deck under constant velocity.

2.2 Computation of flutter speed based on quasi-steady theory
Fully-computational approach of flutter velocity computation permits the substitution of wind tunnel tests by equivalent numerical simulations [18]. This fully computational method is briefly described next.

Scanlan and Tomko [19] established three aeroelastic force components based on frequency dependent function called flutter derivatives as follows.

$$\mathbf{f}_a = \begin{Bmatrix} D_a \\ L_a \\ M_a \end{Bmatrix} = \frac{1}{2}\rho UKB \cdot \begin{pmatrix} P_1^* & -P_5^* & -BP_2^* \\ -H_5^* & H_1^* & BH_2^* \\ -BA_5^* & BA_1^* & B^2 A_2^* \end{pmatrix} \begin{Bmatrix} \dot{v} \\ \dot{w} \\ \dot{\varphi}_x \end{Bmatrix} + \frac{1}{2}\rho U^2 K^2 \cdot \begin{pmatrix} P_4^* & -P_6^* & -BP_3^* \\ -H_6^* & H_4^* & BH_3^* \\ -BA_6^* & BA_4^* & B^2 A_3^* \end{pmatrix} \begin{Bmatrix} v \\ w \\ \varphi_x \end{Bmatrix} \quad (2)$$

where B is the deck width, U is the acting wind speed, $K = B\omega/U$ is the reduced frequency with ω as the response frequency, whereas A_i^*, H_i^* and P_i^* $(i=1,...,6)$ are the flutter derivatives.

The quasi-steady model relates the displacements and rotations of the deck and velocities with the relative wind velocity components. The flutter derivatives may be expressed in terms of force coefficients by comparing the quasi-steady and Scanlan's model as:

$$H_1^* = -\frac{C'_{L,0} + C_{D,0}}{K}; \quad H_2^* = \frac{C'_{L,0} + C_{D,0}}{K} \cdot \mu_H; \quad H_3^* = -\frac{C'_{L,0}}{K^2};$$

$$A_1^* = \frac{C'_{M,0}}{K}; \quad A_2^* = \frac{C'_{M,0}}{K} \cdot \mu_A; \quad A_3^* = -\frac{C'_{M,0}}{K^2} \quad (3)$$

where $C_{L,0}$, $C_{D,0}$, $C_{M,0}$, are lift, drag, and moment coefficients at 0 degree of angle of attack, $C'_{L,0}$, $C'_{D,0}$, $C'_{M,0}$, are their derivatives while μ_H and μ_A can be estimated according to Larose and Livesey [20] as:

$$\mu_H \approx \frac{A_1^*}{H_1^*} \text{ and } \mu_A \approx \frac{A_3^*}{H_3^*}$$

The dynamic equilibrium of a deck under aeroelastic forces, $\mathbf{f_a}$ can be written in a matrix form as:

$$\mathbf{M\ddot{u}} + (\mathbf{C} + \mathbf{C_a})\mathbf{\dot{u}} + (\mathbf{K} + \mathbf{K_a})\mathbf{u} = \mathbf{0} \quad (4)$$

where $\mathbf{M}$, $\mathbf{C}$, and $\mathbf{K}$ are mass, damping, and stiffness matrices, $\mathbf{K_a}$ and $\mathbf{C_a}$ are aeroelastic stiffness and damping matrices. By applying modal analysis to Eq. (4), the solution is a combination of the most relevant m modes. This leads to the following eigenvalue problem:

$$\left(\mathbf{A} - \mu\mathbf{I}\right)\mathbf{w}_\mu e^{\mu t} = 0 \quad (5)$$

where the matrix $\mathbf{A}$ is a function of the matrices, $\mathbf{K_a}$ and $\mathbf{C_a}$, and $\mathbf{w}_\mu$ is an eigenvector. In order to solve this problem, we need mode shapes and natural frequencies of the bridge under study, which can be obtained by a finite element model. The solution to Eq. (5) is expressed as $\mu_j = \alpha_j + i\beta_j$ where α is related to structural damping and β is the damped frequency ($j = 1,... m$ where m is number of frequencies). Flutter occurs when α becomes null with increasing wind speed.

3. CFD analysis of the bridge deck

CFD simulations were performed to obtain force coefficients of the bridge deck for varying shapes. 2D URANS approach was adapted to perform the analyses. The open source CFD code of OpenFoam v.2.4 [21] was used to carry out CFD analyses in this study.

The k-ω Shear-Stress Transport (SST) turbulence model was selected among many available turbulence models because of its good performance and wide acceptance within the bridge engineering field. This model was initially developed by Menter [22] and later improved by Menter and Esch [23]. It takes advantage of robust and accurate formulation of Wilcox k-ω model [24] at the near wall region as well as a good performance of the k-ε turbulence model [25] in the far field. See for example, Sarkic et al. [3], De Miranda et al. [26] and Montoya [27].

In this present work, the bridge planned for crossing of the Julsundet Fjord in Norway is taken as a case study. It is a suspension bridge with a main span of 1.6 km and the deck section is 32 m wide and 4 m high aerodynamic single box girder. The baseline deck geometry in this study follows that of the 1:50 scale model of the planned bridge shown in Figure 2. The further description of the bridge can be found in a report from the Norwegian Public Road Administration [28].

The flow domain and the boundary conditions are illustrated in Figure 3. The flow domain size is $30B$ x $41B$ where B is the deck width. The simulation was performed at Re = 3.5e+5. Uniform velocity of 8 m/s at the inlet boundary was imposed while atmospheric pressure was imposed at the outlet.

Turbulent intensity of 5% was considered for the incoming flow with 0.1 B turbulent length scale. This length scale is also adopted by Ribeiro [29] and Nieto [7]. Both upper and lower walls have slip wall condition while the wall around the deck was non-slip. Linear interpolation of values from cell centres to face centres are carried out. The gradient terms are discretized by the Gauss scheme with linear interpolation. For divergence, the Gauss scheme with linear upwind and the limited linear interpolation schemes were applied. The 2D unstructured mesh was generated using software PointWise [30].
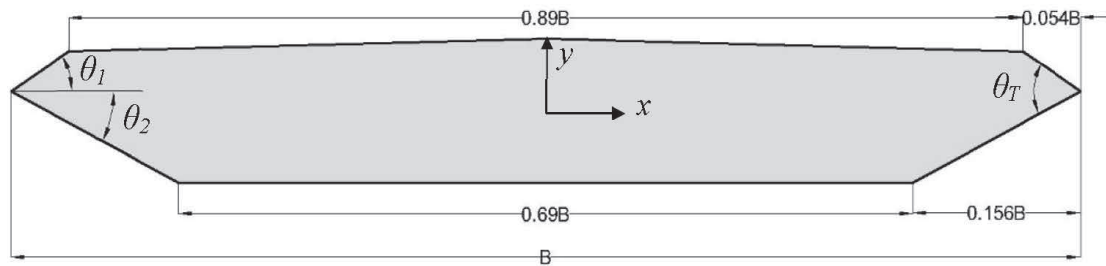
**Figure 2**. Base geometry of the bare deck section.
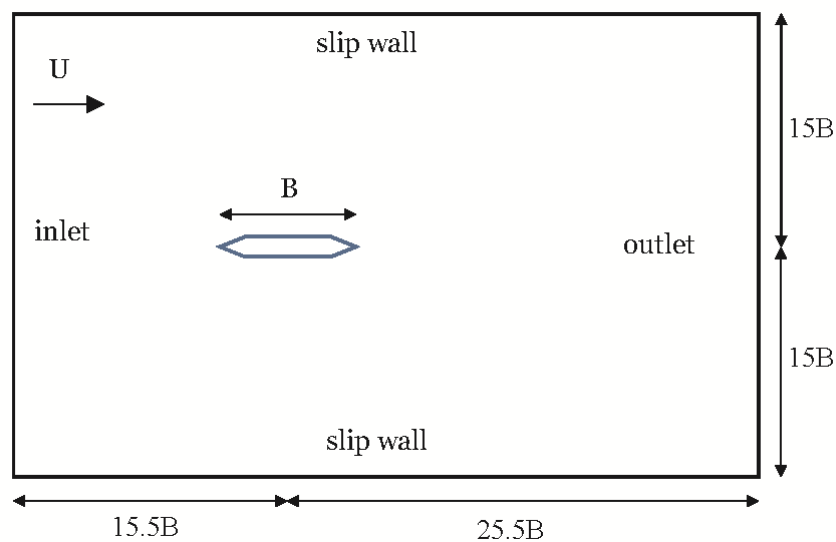
**Figure 3**. Flow domain size and boundary conditions.

A boundary layer mesh was applied around the deck wall in a way that gave a maximum y^+ value less than 4 where $y^+ = u_\tau \cdot h_1 / v = \sqrt{\tau_w / \rho} \cdot h_1 / v$, u_τ is wall friction velocity, h_1, the distance from the wall to the first cell centre, τ_w, wall shear stress, v, kinematic viscosity. The first element height was set to h_1/B=1.14e-4 while Courant number was set to 2 for the simulation time-step. The time integration was verified by Courant number 1 and 0.5 prior to the study, and no significant difference in results were found. A mesh convergence study was conducted using a bare deck section with three different mesh densities in order to verify the discretization. Three types of meshes were considered: a coarse mesh with 112,564 cells, a medium mesh with 196,126 cells and a fine mesh with 321,435 cells. The coarse mesh underestimates the lift coefficient while the medium and fine mesh gave similar results. The medium mesh scheme was therefore selected for the simulations.

3.1 Case study 1

In order to assess the importance of mitigating devices and railings on the force coefficients, the bare deck model with original deck shape in Figure 2 was compared with the model with railings and the mitigating devices shown in Figure 4. The railings geometry is a simplified representation of that adopted in wind tunnel tests [28]. The model has various railings, two guide vanes as well as a spoiler at the bottom center part of the deck. The model scale is 1:50 with respect to the actual bridge dimension of B=32 m. Figure 5 shows the details of mesh for the section with aerodynamic devices. The number of cells for this model is approximately 240,000.
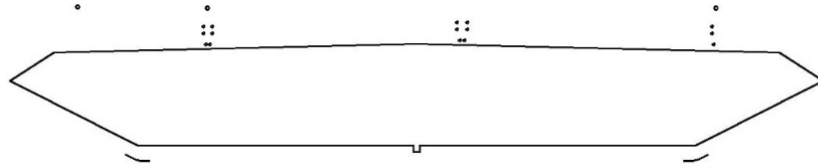
**Figure 4**. Deck geometry with mitigating devices and railings.
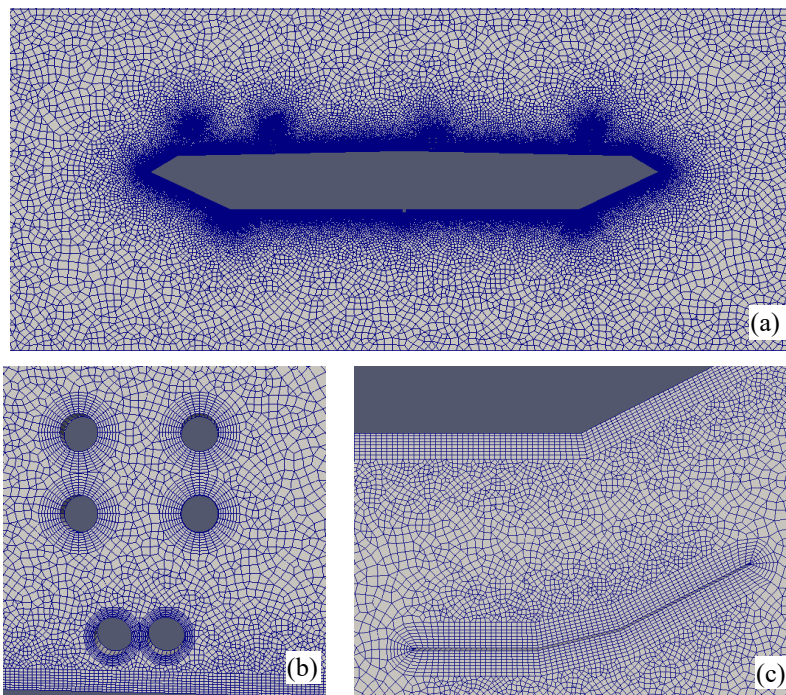
Figure 5. Meshing details of the model (a) with railings (b) and guide vanes (c).

The evaluated force coefficients are summarized in Table 1, along with standard deviation, Strouhal number and the gradient with respect to the angle of attack. Figure 6 shows the force coefficient history of both sections. The bare deck presents periodic oscillations with a single peak frequency while the amplitude of oscillation for the section with mitigating devices are one order of magnitude smaller.

Table 1. Comparison of parameters for the bare deck and the mitigating devices models.

| Geometry	C_L	C_D	C_M	σ_{CL}	σ_{CD}	σ_{CM}	$C_L{'}$	$C_D{'}$	$C_M{'}$	St
Bare deck	-0.00043	0.391	0.0234	0.016	0.0035	0.0034	5.98	0.20	1.45	0.25
Deck & devices	-0.148	0.650	0.0021	0.002	0.0126	0.0005	4.64	0.43	1.29	-
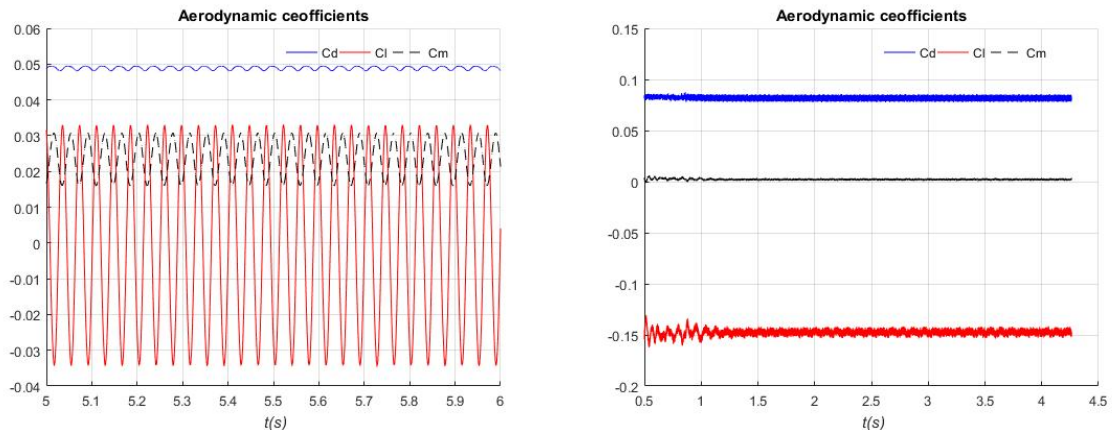
Figure 6. Force coefficients history of bare deck (left) and the section with mitigating devices (right).

Figure 7 shows flow fields for the two cases. The flow field for the bare deck section shows that there is a flow separation at the first corner after the leading edge both at the top and bottom of the deck, but the flow reattaches again close to the edge. From the Figure 7 b1), it is seen that the suction has similar value at the top as well as the bottom plates resulting in overall small lift coefficient. From Figure 7 c1), a vortex shedding phenomenon is clearly observed for this section, which is verified by the standard deviation of the force coefficients (Table 1).

On the other hand, the flow for the section with mitigating devices is rather complex due to the elements added to the deck. From the pressure plot, it can be seen that the pressures on the bottom part are largely negative while the top part experiences rather positive because the flow is slowed down by the railings. This results in a large negative lift coefficient. The vortex shedding behaviour seen for the bare deck section is suppressed for the deck with mitigating devices as could be expected.

The drag coefficient for the section with devices is 66% higher than for the bare deck section because of the various railings and mitigating devices while the moment coefficients are much smaller. The most notable difference is the lift coefficients; -0.00043 for the bare deck and -0.148 for the section with aerodynamic devices. The gradient of the lift coefficient with respect to the angle of attack is 22% smaller for the section with devices, which is favourable for the aerodynamic response of the bridge deck.
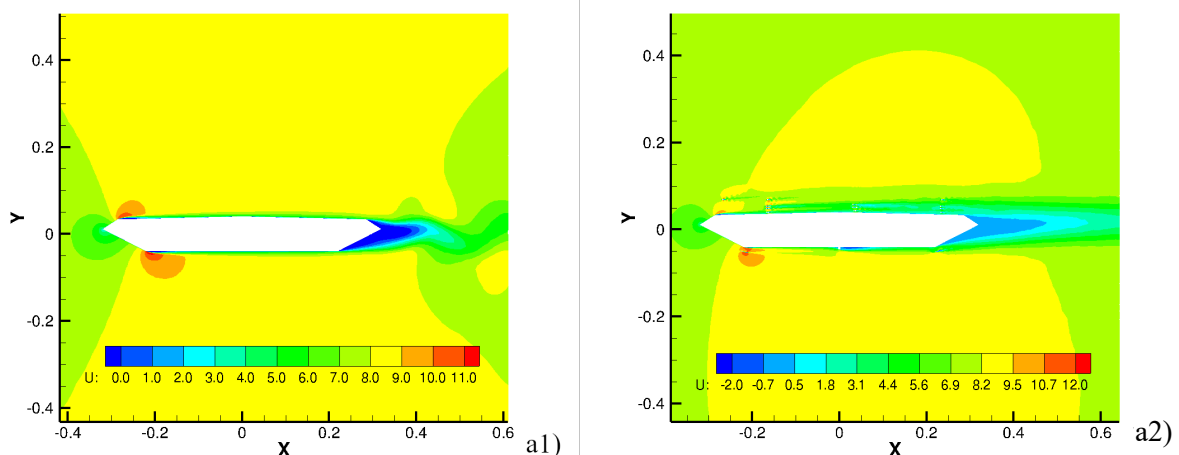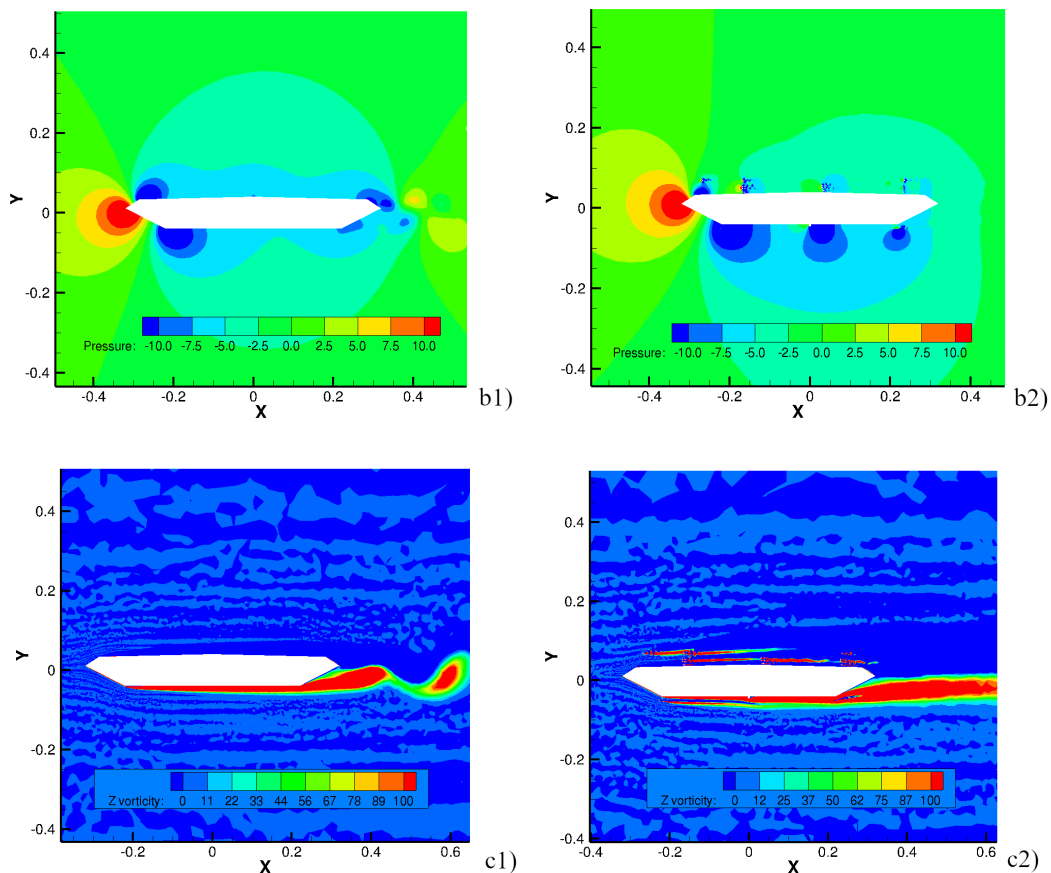
Figure 7. Comparison of instantaneous flow fields of the bare deck (left) and the section with mitigating devices (right): a) velocity *Ux* (m/s), b) pressure (range -10 to +10 Pa) c) z vorticity.

The corresponding force coefficients obtained in the wind tunnel tests are C_D=0.967, C_L=-0.309, C_M=-0.017, C_L'=3.624, C_M'=1.182 [28]. The difference between the simulation and the experimental results is considered primarily due to a higher density of railings on the section model in the experimental set up. Experimental results for another aerodynamic box girder [28] with depth to width ratio of 1:6.2 and similar railing configurations as Julsundet Bridge gave C_D =0.360 for the bare deck and C_D =0.845 for the same section with guard rails. Our drag coefficient for the bare deck model is comparable to these results and the simulation for the section with devices can be improved by additional details of the railings. On the other hand, the objective of this work is a parametric study of a deck section, in which aerodynamic response of the deck is studied for varying the deck width. This concept is later used as a part of multi-fidelity optimization of deck shape considering aerodynamic constraints.
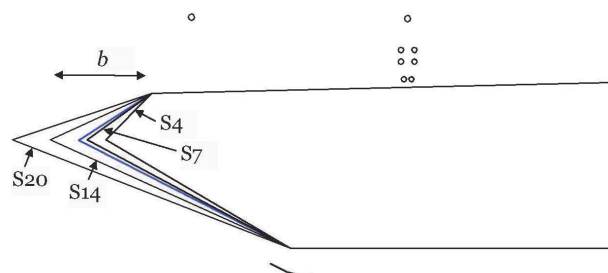
3.2 Case study 2
In this Case study, we have investigated the influence of changing the deck width on the force coefficients while maintaining the deck height. The section with railings and mitigating devices is used for this parametric study. As we change the deck width, we are also changing the angles of the leading and trailing edges. We have considered four cases besides the original design, whose geometries are illustrated in Figure 8 and summarized in Table 2. Each geometry is expressed in terms of a non-dimensional width, $b/0.5B_0$, where b is the horizontal distance from the leading edge to the upper left corner of each deck geometry (Figure 8) and B_0 is the initial deck width.

Table 2. Geometrical properties of the simulations (See Figure 2 for the description of θ_1, θ_2, θ_T).

s. num	$b/0.5B_0$	θ_1	θ_2	θ_T
0	0.121	33	27	60
4	0.076	46	30	70
7	0.107	36	28	64
14	0.168	25	24	49
20	0.231	19	21	40

Figure 8. The deck shapes considered in case study 2 (the blue line shows the original design, s_0).

The force coefficients obtained for different deck shapes are summarized in Table 3 and plotted with respect to the nondimensional width in Figure 9. The lift and moment coefficients refer to the deck width considered in each case. Examples of the evaluated flow fields are shown in Figure 10 for the two extreme section shapes, s_4 and s_{20}.

For the most bluff section of $s4$, a large flow separation is observed because of the large angle of the leading edge, while for the most aerodynamic section of s_{20}, the flow is more attached to the deck. Large negative pressure is observed on the top left corner of the section $s4$, which makes the lift coefficient smaller compared to that of section s_{20}.

As the deck width increases and the leading-edge angle decreases, the lift coefficient and the moment coefficient decrease. The drag coefficient is also slightly reduced with decreasing leading-edge angle. The reduction in the gradient of the lift coefficient is most notable with increasing deck width.

**Table 3.** Force coefficient results of different geometries

| geometry	$b/0.5B_0$	C_L	C_D	C_M	$C_L{}'$	$C_M{}'$
s4	0.076	-0.120	0.650	0.0090	5.67	1.36
s7	0.107	-0.138	0.643	0.0043	4.55	1.23
s14	0.168	-0.164	0.650	-0.0003	3.98	1.22
s20	0.231	-0.181	0.638	-0.0023	3.23	1.17

4. Computation of flutter velocity based on quasi-steady theory

From the force coefficients obtained in the CFD simulations for different deck sections, flutter derivatives were computed based on quasi-steady formulation. Four of the most important flutter derivatives, A_2, A_3, H_2, H_3 are plotted for the sections, $s4$, $s0$ and $s20$ in Figure 11. Other sections are omitted for clarity of representation. For A_2 and A_3 flutter derivative, the gradient $C_M{}'$ is one of the key parameters and for A_2, the ratio of the gradient $C_M{}'/C_L{}'$ is important. On the other hand, for H_2 and H_3, the gradient, $C_L{}'$ is the dominating parameter.
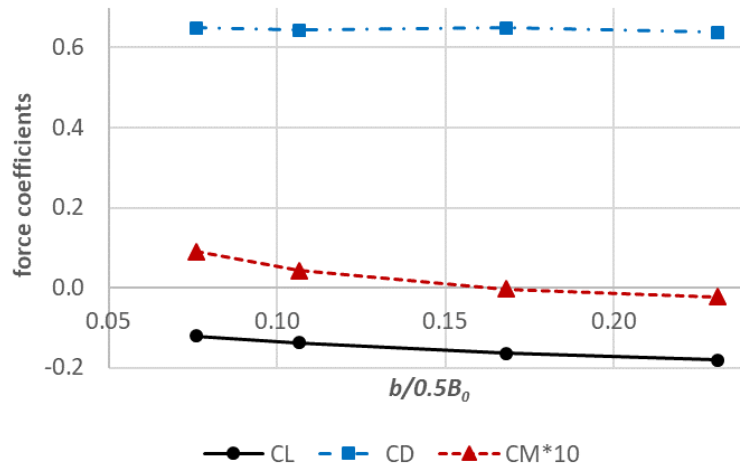
Figure 9. Force coefficients vs nondimensional width $b/0.5B_0$ (C_M is multiplied by 10).
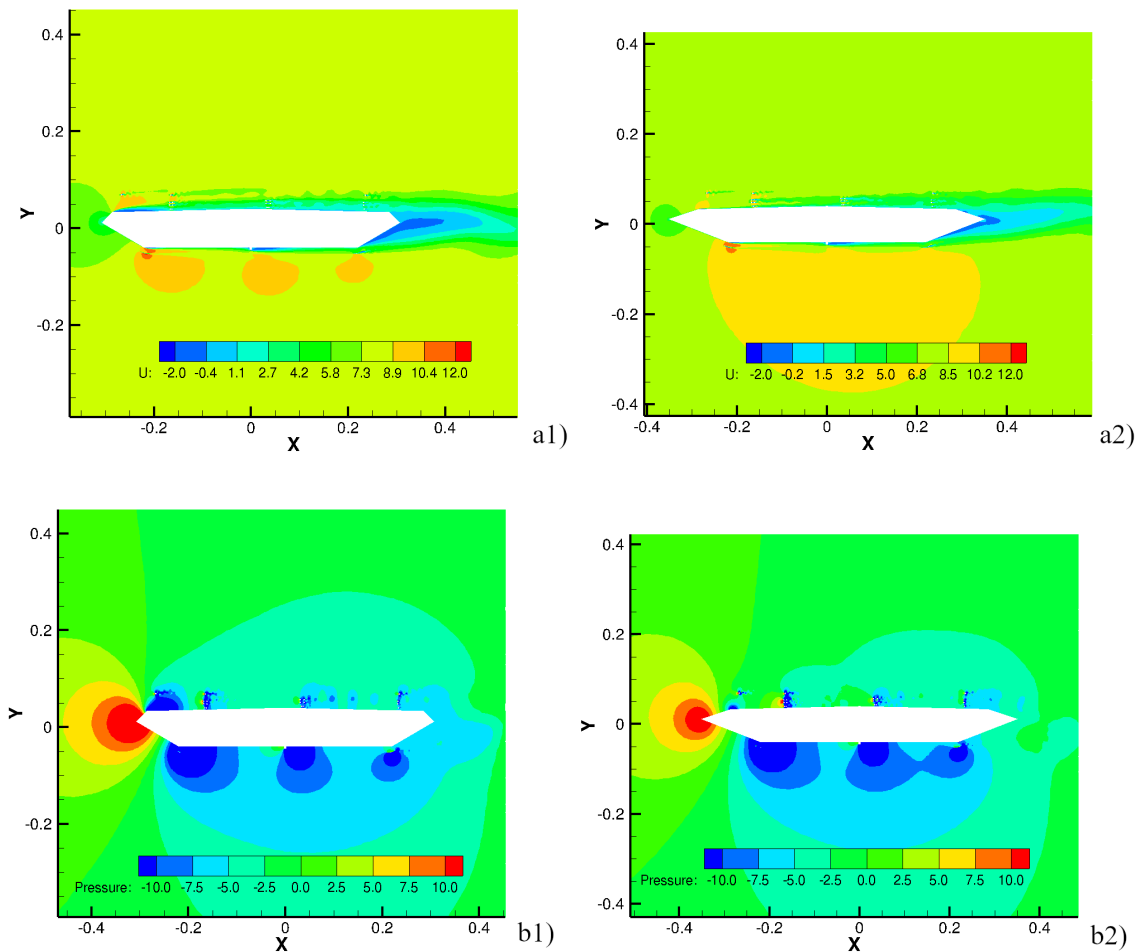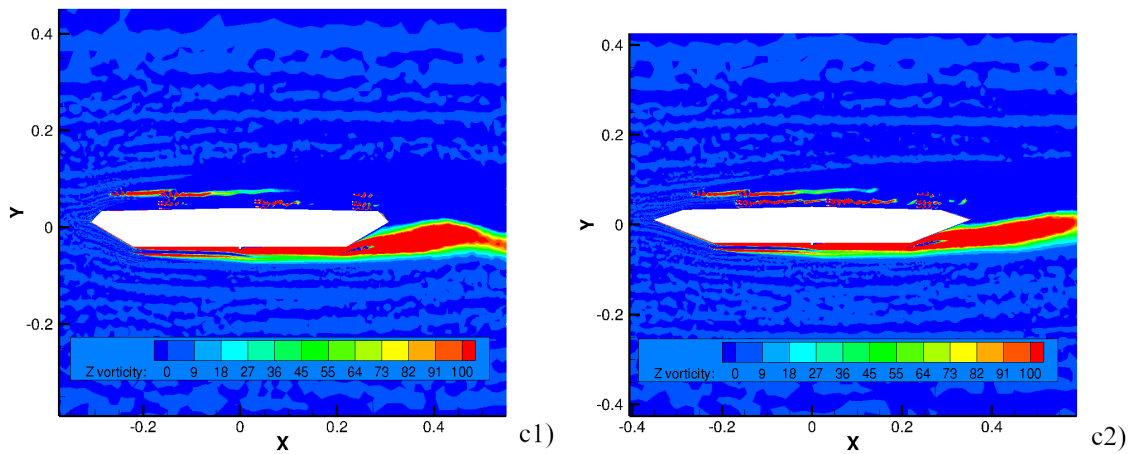
Figure 10. Instantaneous flow fields of *s4* (left) and *s20* (right): a) velocity *Ux* (m/s), b) pressure (range -10 to +10 Pa) c) z vorticity

Flutter velocity of different sections was computed using the first and the second vertical symmetric and the first torsional modes, which are 0.121 Hz, 0.166 Hz and 0.255 Hz respectively [28]. The structural damping ratio was assumed to be 0.3% [31]. The resulting flutter velocity and the corresponding reduced frequency for each section is summarized in Table 4. The flutter velocity of the original design section *s0* is 68.95 m/s, which is similar to the experimental results of 71 m/s [28]. As the deck width increases and the deck shape becomes more aerodynamic, flutter velocity increases. Although the vortex mitigating devices such as guide vanes and spoiler are primarily used to suppress vortex shedding, they also contribute favorably to increase flutter velocity by altering the flow field around the deck.
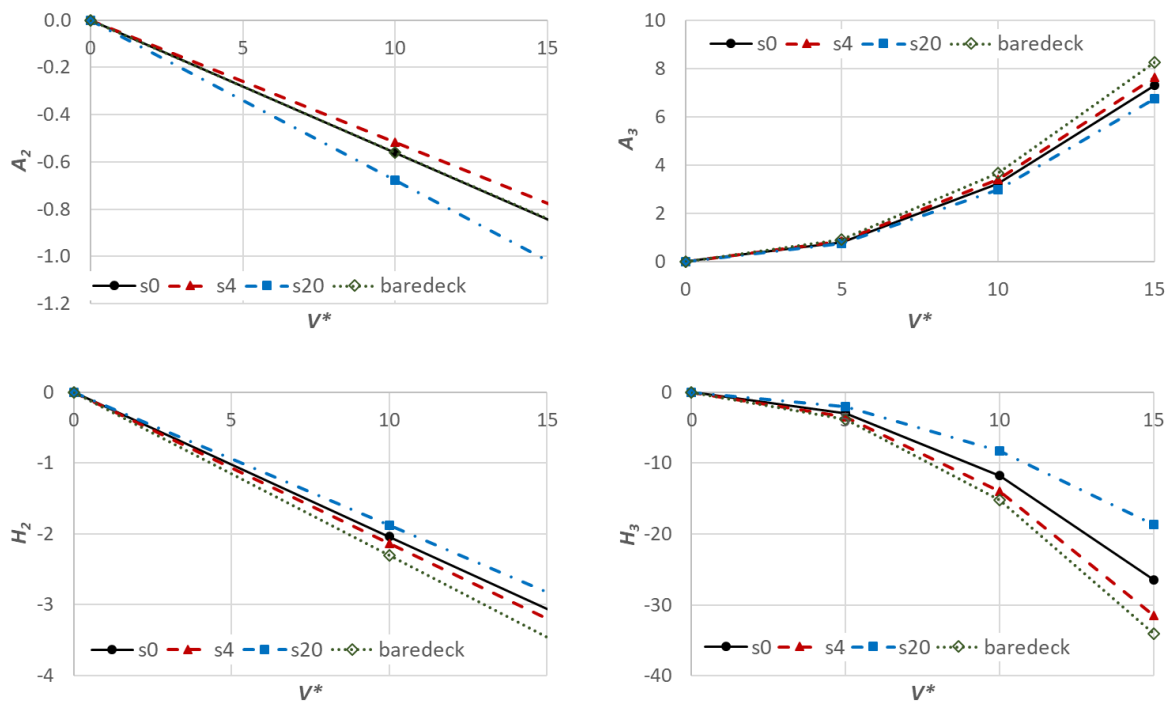
Figure 11. Flutter derivatives, A_2, A_3, H_2 and H_3 for different bridge sections.

Table 4. Flutter velocity V_f and the corresponding reduced frequency K for different deck sections.

geometry	s4	s7	s0	s14	s20	bare deck
$b/0.5B_0$	0.076	0.107	0.121	0.168	0.231	0.121
V_f (m/s)	63.44	67.71	68.95	75.39	79.82	61.21
K	0.68	0.62	0.60	0.52	0.46	0.71

5. Conclusions

CFD analysis of a single-box deck section was carried out to study the importance of railings and vortex mitigating devices on the bridge response under wind loading. Different deck sections were studied such as a bare deck section and sections with mitigating devices and varying deck width. Aerodynamic force coefficients obtained by CFD simulations were then used to compute flutter derivatives based on quasi-steady formulation. Flutter velocity of different sections was calculated for different sections. The section with the largest width to depth ratio has the best performance against flutter instability, while it is seen that the vortex mitigating devices tend to improve the aerodynamic response of the bridge by altering the flow field around the deck. This CFD study will be used as a part of multi-fidelity optimization of a bridge deck shape considering aerodynamic constraint.

Acknowledgement

References

[1]   Gimsing NJ and Georgakis CT 2011 *Cable suppered bridges: concept and design*. Wiley Inc.
[2]   Mannini C, Soda A, Vob R, and Schewe G 2010 Unsteady RANS simulatios of flow around a bridge section. *J. Wind Eng. Ind. Aerod.* **98** 742-53.
[3]   Sarkic A, Fisch R, Hoffer R, and Bletzinger K 2012 Bridge flutter derivatives based on computed, validated pressure fields. *J. Wind Eng. Ind. Aerod.* **104-106** 141-51.
[4]   Ge YJ and Xiang HF 2008 Computational models and methods for aerodynamic flutter of long-span bridges. *J. Wind Eng. Ind. Aerod.* **96** 1912-1924.
[5]   Vairo G 2003 A numerical model for wind loads simulation on long-span bridges. *Simulat. Model. Pract.Theor.* **11** 5-6, 315-51.
[6]   Brusiani F, de Miranda S, Patruno L Ubertini F and Vaona P 2013. On the evaluation of bridge deck flutter derivatives using RANS turbuelnce models. *J. Wind Eng. Ind. Aerod.* **119** 39-47.
[7]   Nieto F, Owen JS, Hargreaves DM and Hernandez S 2015 Bridge deck flutter derivatives: efficient numerical evaluation exploiting their interdependence, *J. Wind Eng. Ind. Aerod.* **136** 138-50.
[8]   Wu T and Kareem A 2013 Bridge aerodynamics and aeroelasticity: a comparios of modelling schemes. *J. Fluid Struct.* **43** 347-70.
[9]   Tubino F 2005 Relationships among aerodynamic admittance functions, flutter derivatives and static coefficients for long-span bridges. *J. Wind Eng. Ind. Aerod.* **93** 929-50
[10]   Jeong W, Liu S, Jakobsen JB and Ong MC 2019 Unsteady RANS simulations of flow around a twin-box bridge girder cross section. *Energies*. **12**(14) 2670.
[11]   Naimul H, Katsuchi H, Yamada H and Nishio M 2015 Flow field analysis of a pentagonal-shaped brige deck by unsteady RANS. *Eng. Appl. Comput. Fluid Mech*. **10**(1) 1-16
[12]   Alvarez AJ, Nieto F and Hernandez S 2019 CFD based study on the effect of aerodynamic appendages in the aerodynamic response of a twin-box deck. 2nd National conference on wind

engineerng, Bucharest, Romania.

[13] Sarwar MW and Ishihara T 2010 Nuerical study on suppresion of vortex-induced vibrations of box girder bridge section by aerodynamic coutermeasures. *J. Wind Eng. Ind. Aerod.* **98** 701-11.

[14] Watanabe S and Fumoto K 2008 Aerodynamic study of slotted box girder using computational fluid dynamics. *J. Wind Eng. Ind. Aerod.* **96** 1885-94.

[15] Cobo del Arco D and Aparicio AC 1999 Improving suspension bridge wind stability with aerodynamic appendages. J. Struct. Eng. **125** 1367-75.

[16] Wilde K, Omenzetter P. and Fujino Y 2001 Suppression of bridge flutter by active deck-flaps control system. *J. Eng. Mech.* **127** 1 80-89

[17] Wang Q, Liao H, Li M and Ma C 2011 Influence of aerodynamic configuration of a streamline box girder on bridge flutter and vortex-induced vibration. *J. Modern Transp.* **19** 261-67.

[18] Larsen A and Walther JH 1998 Discrete vortex simulation of flow around five generic bridge deck section. *J. Wind Eng. Ind. Aerod.* **77–78** 591–602.

[19] Scanlan RH and Tomko JJ 1971 Airfoil and bridge deck flutter derivatives. *J. Eng. Mech. Div.* **97**(6), 1717–37.

[20] Larose, G.L., Livesey, F.M., 1997. Performance of streamlined bridge decks in relation to the aerodynamics of a flat plate. *J. Wind Eng. Ind. Aerod.* **69–71** 851– 60.

[21] OpenFoam Foundation Ltd, 2015. OpenFoam user guide.

[22] Menter F 1994 Two-equation eddy viscousity turbulence models for engineering applications. *AIAA J.* **32(8)** 1598-605.

[23] Menter F and Esch T 2001 Elements of industrial heat transfer prediction. Sixteenth Brazilian congress of mechanical engineering

[24] Wilcox DC 1988 Reassessment of the scale-determining equation for advanced turbulence models. *AIAA J.* **26**(11) 1299-310

[25] Wilcox DC 2006 *Turbulence modelling for CFD*. Third ed. DCW industries Inc, La Canada, CA, USA.

[26] De Miranda M and Bartoli G 2001 Aerodynaic optimization of decks of cable-stayed bridges. Cable-supported bridges-challenging technical limits, procecddings of IASBE conference.

[27] C. Montoya M, Nieto F, Hernandez S, Kusano I, Alvarez AJ and Jurado JA 2018 CFD-based aeroelastic characterization of streamlined bridge deck cross sections subject to shape modifications using surrogate models. *J. Wind Eng. Ind. Aerod.* **177** 405-28.

[28] Norwegian Public Road Administration, 2015. Forprosjekt Hengebru over Julsundet. technical report.

[29] Ribeiro AFP 2011 Unsteady RANS modelling of flow past a rectangular 5:1 cylinder: investigation of edge sharpness effects. 13th Int'l conference on wind engineering

[30] PointWise Inc. 2018. version 18.1 R2

[31] Caetano E 2015 Innovative Bridge Design Handbook. Alessio Pipinato.